

PAPER • OPEN ACCESS

## Negative differential resistance effect of blue phosphorene-graphene heterostructure device

To cite this article: Si-Cong Zhu *et al* 2020 *J. Phys. Commun.* **4** 035005

View the [article online](#) for updates and enhancements.



## PAPER

## Negative differential resistance effect of blue phosphorene-graphene heterostructure device

## OPEN ACCESS

## RECEIVED

14 November 2019

## REVISED

24 February 2020

## ACCEPTED FOR PUBLICATION

27 February 2020

## PUBLISHED

9 March 2020

Original content from this work may be used under the terms of the [Creative Commons Attribution 4.0 licence](#).

Any further distribution of this work must maintain attribution to the author(s) and the title of the work, journal citation and DOI.



Si-Cong Zhu<sup>1,2,5</sup> , Tie-Yi Hu<sup>1</sup>, Kai-Ming Wu<sup>1</sup>, Chi-Hang Lam<sup>2</sup>, Kai-Lun Yao<sup>3</sup>, Hua-Rui Sun<sup>4</sup>  and Cho-Tung Yip<sup>4,5</sup>

<sup>1</sup> The State Key Laboratory for Refractories and Metallurgy, Hubei Province Key Laboratory of Systems Science in Metallurgical Process, Collaborative Innovation Center for Advanced Steels, International Research Institute for Steel Technology, Wuhan University of Science and Technology, Wuhan 430081, People's Republic of China

<sup>2</sup> Department of Applied Physics, Hong Kong Polytechnic University, Hung Hom, Hong Kong, People's Republic of China

<sup>3</sup> Wuhan National High Magnetic Field Center and School of Physics, Huazhong University of Science and Technology, Wuhan 430074, People's Republic of China

<sup>4</sup> Department of Physics, Shenzhen Graduate School, Harbin Institute of Technology, Shenzhen 518055, People's Republic of China

<sup>5</sup> Authors to whom any correspondence should be addressed.

E-mail: [sczhu@wust.edu.cn](mailto:sczhu@wust.edu.cn) and [h0260416@hit.edu.cn](mailto:h0260416@hit.edu.cn)

**Keywords:** blue phosphorene, graphene, heterostructure, negative differential resistance, first principles

### Abstract

We report on the electrical transport properties of new graphene/blue phosphorene heterostructure devices by density functional theory (DFT) within the non-equilibrium Green's function (NEGF) approach. From the results, it is found that the devices with different length of contacts layers show semiconducting nature. The integrated contacted length of graphene/blue phosphorene two-layer device shows the best conductivity under a bias voltage. The negative differential resistance effect (NDR) is also found in the current-voltage curve of all the graphene/blue phosphorene devices. Transport characteristics can be explained by the eigenvalues of self-consistent Hamiltonian (MPSH). The results show that the device is fabricated from graphene/blue phosphorous and has good electrical conductivity. These interesting features will be useful for future electronic products.

## 1. Introduction

Schottky junction is one of the basic components used in rectifier, diode, transistor, photoelectric and photodetector device in electronics and optoelectronics [1]. Nowadays, with advanced fabrication technology, we can make those electronic devices to be atomic thin. Those ultra-small size devices also trigger further research on new quantum behaviors at the atomic scale. In recent years, due to the outstanding electronic properties, graphene has attracted considerable research interest in future electronic applications. However, due to the gapless nature of graphene, this hinders of its application modern electronic devices that require finite band gap, i.e., field-effect transistor, light-emitting diode, etc. Graphene integration in heterogeneous junctions has been reported that there is a small gap in the Dirac cone with tens of MeV in it [2–5]. Therefore, graphene semiconductor junction (GSJ) can open up band gap, and it had been realized to be an effective rectifier, chemical sensor, a solar cell [6]. By applying an external electric field and intentional doping, various Schottky barriers of GSJ can be achieved [7, 8]. Furthermore, that GSJ can also integrate to other 2D semiconductors to form different heterojunctions such as graphene–hBN [9, 10], graphene–MoS<sub>2</sub> and also graphene–black phosphorus [11–14].

Although GSJ can make graphene to be gapless, it still has a great demand to have alternative 2D semiconductors having both high mobility and finite band gap for the applications of electronics. Blue phosphorus (BlueP) and black phosphorus [15–23], which have both ultra-high mobility and finite band gap (2.0 eV and 0.5 eV, respectively), can satisfy the above mentioned properties [24]. Theoretical computations with external stimuli such as application of an electric field and surface functionalization [25] on the electronic properties of BlueP have also been conducted to explore the effects of doping [26–29]. Recently, the BlueP has

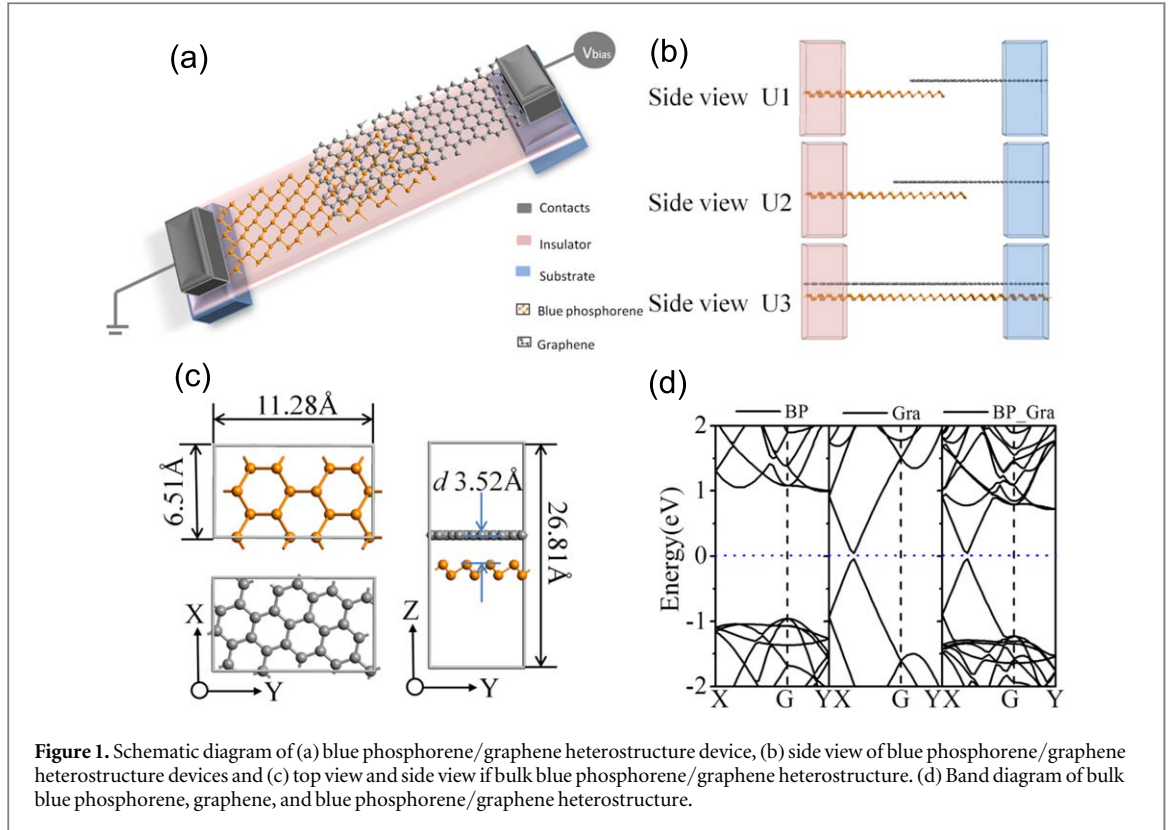


**Figure 1.** Schematic diagram of (a) blue phosphorene/graphene heterostructure device, (b) side view of blue phosphorene/graphene heterostructure devices and (c) top view and side view if bulk blue phosphorene/graphene heterostructure. (d) Band diagram of bulk blue phosphorene, graphene, and blue phosphorene/graphene heterostructure.

been successfully synthesized by epitaxial growth on different substrates [30, 31]. It is believed that by integrating the BlueP with other 2D materials, we can get a new type of heterostructure for future applications. Here we report the electronic properties of a graphene/BlueP Schottky junction heterostructure by first principles. We calculate the electrical transport of different length for graphene/BlueP heterostructure devices. The negative differential resistance (NDR) effect is observed in the electron current of all the graphene/blue phosphorene devices.

## 2. Results and discussion

The model device displayed in figure 1(a) is formed from three parts: the scattering region, the right, and left electrodes. A  $4 \times 4$  supercell model of blue phosphorene contacted with graphene is built. Here, we label the device with the symbol U1-U3 for different contacted lengths of BlueP and graphene in the scattering region, as shown in figure 1(b). The contact lengths of central scattering region for U1, U2 and U3 are 8.86 Å, 18.6 Å and 45.1 Å. The bilayer devices with different scattering regions are set as single- $\zeta$  polarization as implemented in software of ATK [32–34] which is simulated employment the density function theory (DFT) with the nonequilibrium Green's function (NEGF) method. By using the Perdew-Burke-Ernzerhof (PBE) and generalized gradient approximation (GGA), we calculate the extend valence electron orbitals and the exchange correlation potential. Meanwhile, local density approximation (LDA) and Perdew–Burke–Ernzerhof (PBE) is used to calculate, and very similar results are obtained. The electronic current dependent of bias through the system is calculated by Landauer formula:

$$J = \int_{-\infty}^{\infty} T(E)[f(E, \mu_L) - f(E, \mu_R)]dE \quad (1)$$

Where  $\mu_{L,R}$  is the electrochemical potentials for the left or right electrode by the Fermi energy  $E_f$ , and  $f(E, \mu_{L,R})$  is equilibrium Fermi distribution of the left or right electrode, and the transmission  $T(E)$  is defined as:

$$J = T(E) = Tr[\Gamma_L G^R \Gamma_R G^A] \quad (2)$$

Where  $\Gamma_{L(R)}$  is the coupling matrix for the left or right electrode, and  $G^{R(A)}$  is the retarded Green's functions for the central scattering region. The system was relaxed sufficiently till the maximum force dropped below a threshold value  $0.05 \text{ eV \AA}^{-1}$ .

We studied the transport characteristics of the heterostructure of BlueP/graphene. The device structure is shown in figure 1(a), where the central region is the scattering region and the right and left electrodes are semi-infinite structures. The electron transport direction of the device is from left to right, and its temperature is set at

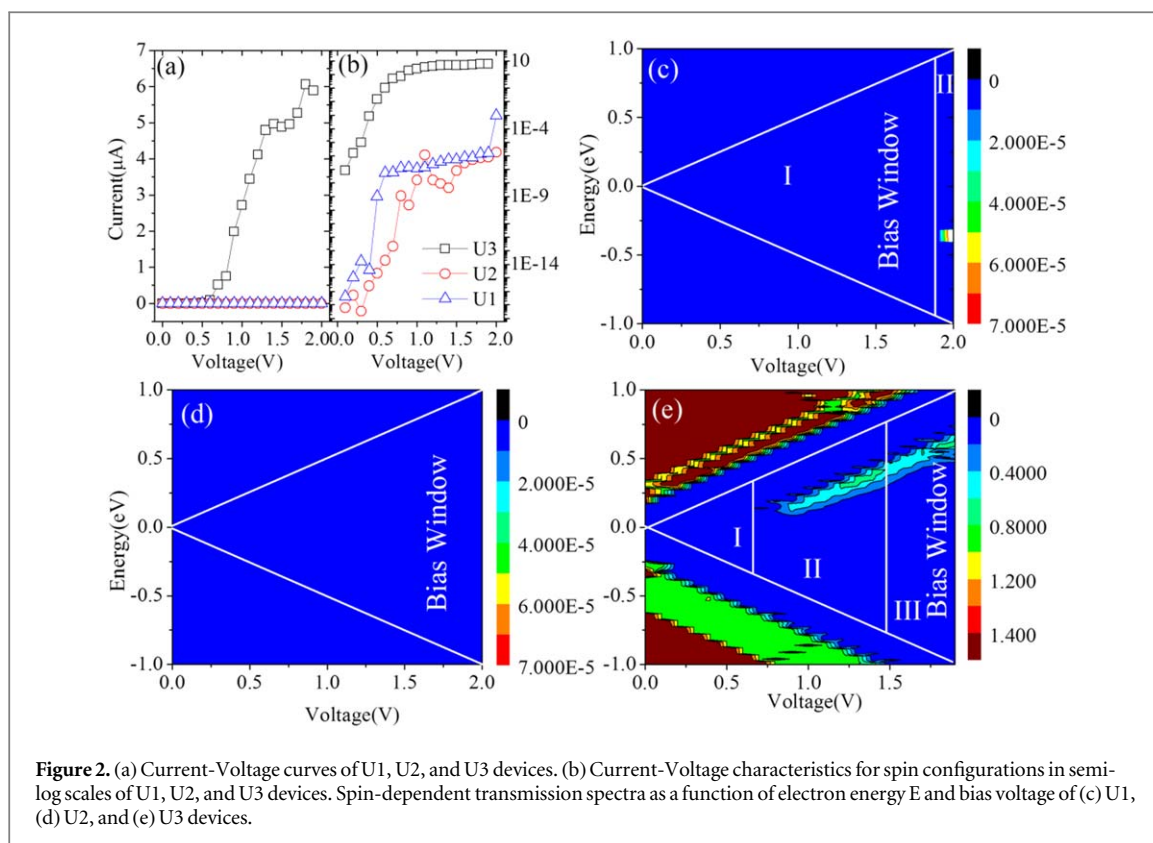


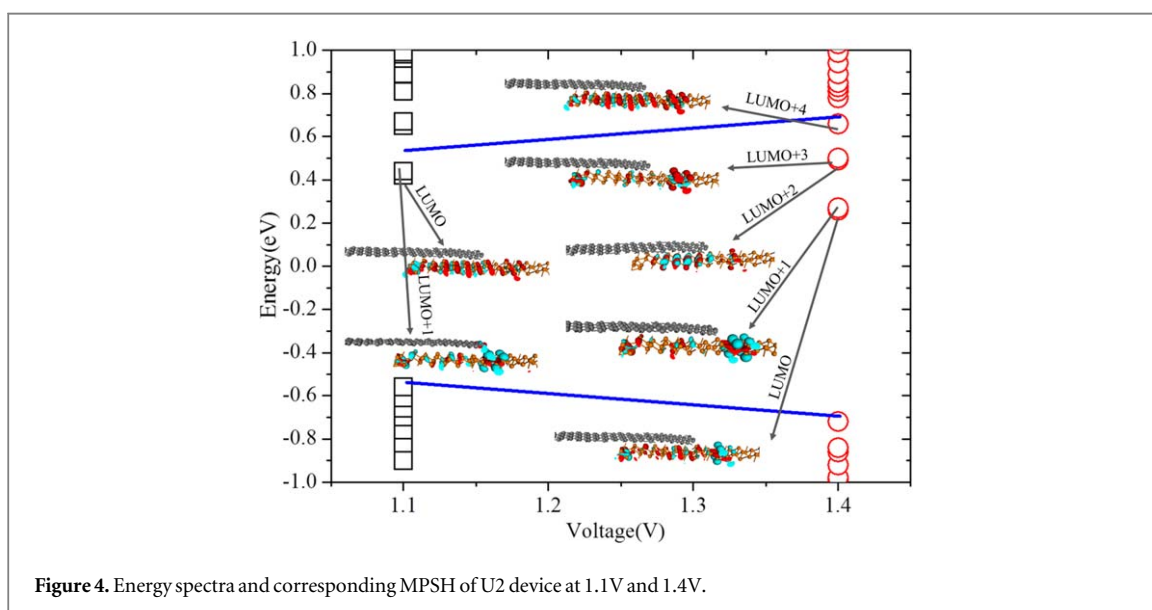
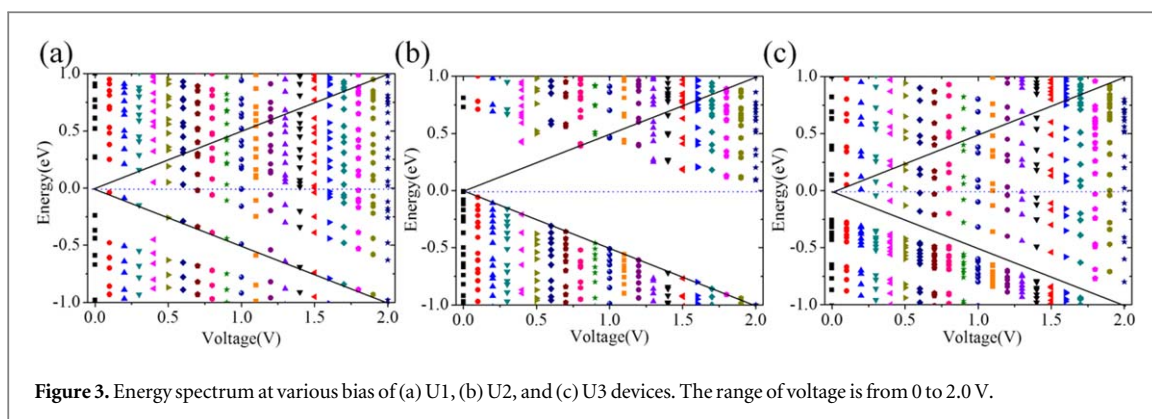
**Figure 2.** (a) Current-Voltage curves of U1, U2, and U3 devices. (b) Current-Voltage characteristics for spin configurations in semi-log scales of U1, U2, and U3 devices. Spin-dependent transmission spectra as a function of electron energy  $E$  and bias voltage of (c) U1, (d) U2, and (e) U3 devices.

300 k. The whole device, including lead and scattering region, is non-polarized. The simulated current-voltage (I-V) curves of blue phosphorene/graphene devices are shown in figure 2(a) respectively. In figure 2(a), the IV curve of U3 shows typical transport properties as a semiconductor and when the bias voltage reaches 0.6 V, the current turn on. When the bias voltage increases from 0.6V to 1.1V, the current increases rapidly. Furthermore, when the bias voltage is higher than 1.1V, the current is decreased, correspondingly. A negative differential effect (NDR) peak is obtained at the 1.1V, while another NDR peak is observed at 1.8V bias voltage. Meanwhile, the currents of U1 and U2 are much lower than the U3 device. The I-V characteristics for U1, U2, and U3 devices in semi-log scales are shown in figure 2(b). The results show that U1 current is 10 orders of magnitude larger than U2 and U3 at low bias. As figure 2(b) shown, for the U1 and U2, there are threshold voltages at about 0.6 V and 0.8V, which are induced by the band gap of the left electrode in the band structure (figure 1(d)). When the bias voltage is increased continuously, the currents for the two devices are rapidly increasing. Furthermore, there are three NDR peaks appear for U2 in bias voltage 0.1V, 0.8V, and 1.1V.

To further understand the transmission mechanism in the device structures, we calculate the transmission spectra of U1, U2 and U3 devices as a function of bias voltage and electron energy  $E$ . The transmission spectra of the U1, U2, and U3 devices are shown in figures 2(c)–(e). In U1 state, when the bias voltage is more than 1.9v, the transmission peak enters the bias window (BW) (region II), leading to a rapidly increasing of current as shown in figure 2(b). In the U2 state, no transmission peak appears in the BW, leading to the suppression of current. In U3 state, when the bias voltage is lesser than 0.6v, there is no transmission peak in the BW (Region I). Whereas, When the bias voltage is greater than 0.6v, transmission peak appears in the BW, leading to a rapidly increase of the current (in U3 device of figure 2(a)). When the bias is increased further, there is a transmission peak at the bias voltage of 1.4V, a little part of the transmission spectra enter the BW (region II), and the displacement of the transmission peak is less obvious in region III. The current decreases when there is a NDR peak. In the U3 device, the transmission spectra are much larger than those of U2 and U3 ones, causing the much more order of magnitude for current (In figure 2).

Therefore, the current of the U3 device is larger than that of U2 and U3. Since the current-voltage curves display NDR behavior, which is very useful for the applications of electronics devices. From figures 3(a)–(c) shown, the black triangle is the bias window, one can see that by enhancing the direct voltage from 0 V to 2.0 V, the energy spectra for U1, U2, and U3 scattering regions shift to lower energy. The energy gap of U2 is much larger than the other two, leading to the lowest current value. When the bias voltage reaches 0.6V, the LOMO enters the bias window, and then the current of U1 device shows the ‘on’ state in figure 3(a).

The conductivity of the bilayer heterostructure depends not only on the energy of the molecular orbitals near the Fermi level, but also on the spatial distribution of the frontier molecular orbitals. To understand the physics



of these transmission peaks of NDR in  $E_f$  and its variation with bias changes, we calculate the molecular spatial distribution prediction with the molecular projected self-consistent Hamiltonian (MPSH) eigenvalues contributing to the current integral for 1.1V and 1.4V U2 devices.

The spatial contribution of these MPSH eigenstates are shown in figure 4, all the MPSH states are located at blue phosphorus, for 1.1V: LUMO4, and LUMO + 1, for 1.4V: LUMO, LUMO + 1, LUMO + 2, LUMO + 3 and LUMO + 4, which are all in the bias window. From the results show that at bias voltage 1.1V, the LUMO, and LUMO + 1 MPSH states are delocalized for the transition direction. The spatial contributions of LUMO, LUMO + 1, LUMO + 2 and LUMO + 3 are localized, while the bias voltage increases to 1.4V. Before all, the molecular orbital state of P atom is significantly reduced which is in the scattering region of the device. Only the LUMO + 4 shows delocalized characteristic along the transition direction. Reduction and localization weaken U2's scattering region coupling between graphene and BlueP, and electrons through the device from one layer can't quit the layer again to get to another layer. In result, the transmission through the U2 heterostructure is suppressed, while the current is decreased correspondingly. The current of U2 device thus shows significant negative differential resistance effect (NDR).

### 3. Conclusions

In conclusion, a new configuration for bilayer heterostructure device based on graphene and blue phosphorus is presented, and its electrical transport properties have been investigated by NEGF-DFT approach. The interesting voltage-current effect can be produced only by applying the bias voltage between the left and the right electrodes of three different contacted lengths of graphene/BlueP scattering region. The U3 device shows the highest current among all the devices. The NDR effect is observed in all the devices. It is expected that this graphene/blue phosphorus-based materials based device can achieve some interesting properties, which can be used for future electronics.

## Acknowledgments

Si-Cong Zhu, Shun-Jin Peng, Kai-Ming Wu, Chi-Hang Lam and Kai-Lun Yao would like to acknowledge the support from *Hong Kong Scholars Program No.XJ2016007*, National Natural Science Foundation of China under Grants No. 11704291, No.11647047 and No. 11704292, and HK PolyU under Grant No. G-YBHY, and foundation for University Key Teachers from the WUST of No. 2017xz024. Cho Tung Yip and Huarui Sun were supported by grants from Shenzhen Municipal Science and Technology projects (Grant No. JCYJ201803063000421 and No. JCYJ20160531192714636) and Shenzhen Overseas High-Caliber Personnel Technology Innovation Project No. KQJSCX20170726104440871.

## ORCID iDs

Si-Cong Zhu  <https://orcid.org/0000-0003-2103-3998>

Hua-Rui Sun  <https://orcid.org/0000-0003-1429-0611>

## References

- [1] Abergel D S L, Wallbank J R, Chen X, Mucha-Kruczyński M and Fal'ko V I 2013 *New J. Phys.* **15** 123009
- [2] Brandbyge M, Mozos J-L, Ordejón P, Taylor J and Stokbro K 2002 *Phys. Rev. B* **65** 165401
- [3] Cai Y, Zhang G and Zhang Y-W 2015 *J. Phys. Chem. C* **119** 13929–36
- [4] Fiori G, Samantha B and Giuseppe I 2012 *IEEE Trans. Electron Devices* **60** 268–73
- [5] Giovannetti G, Petr A K, Brocks G, Kelly P J and Van Den Brink J 2007 *Phys. Rev. B* **76** 073103
- [6] Guan J, Zhu Z and Tománek D 2014 *Phys. Rev. Lett.* **113** 046804
- [7] Hu W, Wang T and Yang J 2015 *J. Mater. Chem. C* **3** 4756–61
- [8] Jin C, Filip A R and Kristian S T 2015 *J. Phys. Chem. C* **119** 19928–33
- [9] Kiani M J, Ahmadi M T, Abadi H K F, Rahmani M and Hashim A 2013 *Nanoscale Res. Lett.* **8** 173
- [10] Liang J, Bi H, Wan D and Huang F 2012 *Adv. Funct. Mater.* **22** 1267–71
- [11] Liu X and Li Z 2015 *The Journal of Physical Chemistry Letters* **6** 3269–75
- [12] Lu J, Zeng H, Liang Z, Chen L, Zhang L, Zhang H, Liu H, Jiang H, Shen B and Huang M 2015 *Sci. Rep.* **5** 14739
- [13] Ma Y, Dai Y, Wei W, Niu C, Yu L and Huang B 2011 *J. Phys. Chem. C* **115** 20237–41.
- [14] Mogulkoc Y, Modarresi M, Mogulkoc A and Ciftci Y O 2016 *Comput. Mater. Sci.* **124** 23–9
- [15] Nguyen T C, Otani M and Okada S 2011 *Phys. Rev. Lett.* **106** 106801
- [16] Okada S 2010 *Japan. J. Appl. Phys.* **49** 020204
- [17] An Y, Hou Y, Wang H, Li J, Wu R, Wang T, Da H and Jiao J 2019 *Phys. Rev. Appl.* **11** 064031
- [18] An Y, Jiao J, Hou Y, Wang H, Wu R, Liu C, Chen X, Wang T and Wang K 2018 *J. Phys. Condens. Matter* **31** 065301
- [19] An Y, Sun Y, Zhang M, Jiao J, Wu D, Wang T and Wang K 2018 *IEEE Trans. Electron Devices* **65** 4646–51
- [20] Li Y, Ye F, Xu J, Zhang W, Feng P X-L and Zhang X 2018 *IEEE Trans. Electron Devices* **65** 4068–72
- [21] Zhang M, An Y, Sun Y, Wu D, Chen X, Wang T, Xu G and Wang K 2017 *Phys. Chem. Chem. Phys.* **19** 17210–5
- [22] Zhang X 2019 *Adv. Mater. Sci. Eng.* **2019** 1–77865698
- [23] Xiaoyang Z and Xian Z 2019 *Excitons in Two-Dimensional Materials* <https://www.intechopen.com/online-first/excitons-in-two-dimensional-materials> (<https://doi.org/10.5772/intechopen.90042>)
- [24] Novoselov K S, Geim A K, Morozov S V, Jiang D, Zhang Y, Dubonos S V, Grigorieva I V and Firsov A A 2004 *Science* **306** 666–9
- [25] Yu L, Lee Y-H, Ling X, Santos E J G, Shin Y C, Lin Y, Dubey M, Kaxiras E, Kong J and Wang H 2014 *Nano Lett.* **14** 3055–63
- [26] Mohamed S, Sharaf A H, Emira A, Abdul-Wahed A and Gamal A 2015 *Sens. Actuators, A* **232** 329–40.
- [27] Soler J M, Artacho E, Gale J D, García A, Junquera J, Ordejón P and Sánchez-Portal D 2002 *J. Phys. Condens. Matter* **14** 2745
- [28] Sun M, Hao Y, Ren Q, Zhao Y, Du Y and Tang W 2016 *Solid State Commun.* **242** 36–40
- [29] Sun M, Tang W, Ren Q, Wang S-ke, Yu J and Du Y 2015 *Appl. Surf. Sci.* **356** 110–4
- [30] Yu W, Zhu Z, Niu C-Y, Li C, Cho J-H and Jia Y 2016 *Nanoscale Res. Lett.* **11** 77
- [31] Zeng J, Cui P and Zhang Z 2017 *Phys. Rev. Lett.* **118** 046101
- [32] Zhang J L et al 2016 *Nano Lett.* **16** 4903–8
- [33] Zhu L, Wang S-S, Guan S, Liu Y, Zhang T, Chen G and Yang S A 2016 *Nano Lett.* **16** 6548–54
- [34] Zhu S-C, Yip C-T, Peng S-J, Wu K-M, Yao K-L, Mak C-L and Lam C-H 2018 *Phys. Chem. Chem. Phys.* **20** 7635–42